PHYSICAL REVIEW B **79**, 161302(R) (2009)

Probing the impact of microstructure on the electroluminescence properties of Ge-nanocrystal enriched Er-doped SiO_2 layers

A. Kanjilal,* L. Rebohle, N. K. Baddela, S. Zhou, M. Voelskow, W. Skorupa, and M. Helm
Institute of Ion Beam Physics and Materials Research, Forschungszentrum Rossendorf, P.O. Box 51 01 19, 01314 Dresden, Germany
(Received 16 February 2009; published 14 April 2009)

We present the microstructural evolution in Ge-rich SiO_2 doped with Er under different fabrication conditions. At sufficiently high Er contents and annealing temperatures, the Er_2O_3 and $Er_2Ge_2O_7$ phases are eventually formed, leading to an electroluminescence quenching of Ge-related oxygen-deficiency centers. The correlation between the microstructure and electroluminescence is discussed based on: (i) an Er doping dependent fragmentation/amorphization of Ge nanocrystals, (ii) a temperature dependent Ge diffusion toward the Si/SiO_2 interface, and (iii) the formation of different Er phases.

DOI: 10.1103/PhysRevB.79.161302 PACS number(s): 78.67.Bf, 85.60.Jb

The possibility of enhancing the excitation cross section of Er ($\sim 10^{-20}$–10^{-21} cm^2) (Refs. 1 and 2) and improving the 1.53 μm Er photoluminescence[1–3] or electroluminescence (EL) (Refs. 4 and 5) intensity from an Er-doped SiO_2 layer by introducing additional *sensitizers*, especially semiconductor nanocrystals (NCs),[1–3] has extensively been investigated. For instance, optically excited Si NCs (Refs. 1–3) embedded in a SiO_2 layer are able to pump nearby Er^{3+} ions, which subsequently decay radiatively via intra-4*f* ($^4I_{13/2} \rightarrow {}^4I_{15/2}$) transition by emitting light at ~ 1.53 μm.[1] Invariably, excitation cross sections of Er in such system can reach values comparable to those of Si NCs ($\sim 10^{-17}$–10^{-16} cm^2).[2] However, the formation of oxidized Er clusters cannot be avoided due to the low solubility limit of Er^{3+} ($\sim 10^{18}$ cm^{-3}) (Ref. 6) in SiO_2. Usually they grow up in size during postimplantation annealing[7] or by high dose Er implantation[8]—detrimental for the 1.53 μm Er luminescence. It is, therefore, interesting to find an alternative approach to dissolve the Er^{3+} ions.

In the quest for an alternative host material, SiO_2 containing Ge NCs is considered to be one of the possible candidates as Ge NCs are superior to the Si counterpart in terms of quantum confinement,[9] and interband absorption.[10] However, concerning the Er^{3+} pumping, photoexcited Ge nanoparticles are not as effective as Si NCs.[11] Recently, we have investigated SiO_2 layers containing both Ge NCs and Er^{3+} ions[12] and found surprisingly that electrically excited Er^{3+} ions behave like sensitizers for pumping Ge-related oxygen-deficiency centers, GeODCs, called *inverse energy transfer* process, in a metal-oxide semiconductor (MOS) structure. This phenomenon is of special interest for both scientific and application viewpoints, as the understanding of the inverse energy transfer process allows either to avoid it in case of Er-based light emitters or exploit it in case of Ge-based light emitters.

In this Rapid Communication we report on the microstructural evolution in a system such as SiO_2:Ge-NC:Er under different fabrication conditions and correlate these results with the inverse energy transfer process. We show that with increasing annealing temperature, the microstructure will pass through a state of crystalline Er_2O_3 to the $Er_2Ge_2O_7$ phase. In this scenario, the maximum GeODC-based EL yield is achieved prior to the formation of the Er_2O_3 nanocrystallites.

The standard MOS structures were fabricated by local oxidation of silicon (LOCOS) technology with a 200-nm-thick thermally grown SiO_2 layer on *n*-type Si(100) wafers. Initially, 130 keV Ge ions were implanted, with their maximum concentration lying in the range of 3.5 and 11.1% at $R_p \sim 112$ nm as derived from the SRIM-2006 calculations.[13] The samples were furnace annealed at 950 °C for 60 min to produce Ge NCs. Subsequently, 250 keV Er ions were implanted with a maximum concentration between 0.3 and 1.4% at $R_p \sim 115$ nm, followed by annealing at 800–1100 °C for 30 min to remove implantation-induced defects and to activate Er^{3+} ions.[14] About 100-nm-thick silicon-oxynitride (SiON) layer was deposited on top of the LOCOS structure. Semitransparent indium-tin oxide (ITO) and aluminum contacts were sputter deposited on the front and rear surfaces, respectively. The ITO layer was patterned by optical lithography to achieve arrays of circular electrodes (diameter ~ 300 μm).

All samples were studied using synchrotron-radiation x-ray diffraction (XRD) with a 5° grazing incidence of the Cu K_a radiation at the Rossendorf beamline (ROBL) in the European Synchrotron Radiation Facility, Grenoble. Complementary results were obtained from a 532 nm yttrium aluminum garnet (YAG) laser (power on sample surface ~ 2 mW) excited μ-Raman spectra, recorded in the scattering geometry with a liquid-nitrogen-cooled charge-coupled device camera in a Raman microscope. Depth profiles of the implanted elements were examined by Rutherford backscattering spectrometry (RBS). Cross-sectional transmission-electron-microscopy (TEM) images were taken by a FEI Titan 80–300 S/TEM instrument operating at 300 keV. Room-temperature EL spectra were recorded with constant current mode and under forward bias conditions and by a monochromator in combination with a photomultiplier or liquid-nitrogen-cooled InGaAs detector.

Figure 1(a) shows the μ-Raman spectra of the Ge-rich SiO_2 layers containing 3.5–11.1 % Ge, along with a spectrum for bulk crystalline Ge, *c* Ge. The peak at ~ 300.2 cm^{-1} with a full width at half maximum (FWHM) of ~ 3.1 cm^{-1} is the characteristic feature of the Ge-Ge mode of *c* Ge.[15] The spectrum for 3.5% Ge consists of a relatively broad and weak peak at ~ 303.5 cm^{-1} with FWHM ~ 20 cm^{-1}. For 7.4% Ge, the Ge-related peak is not only sharper and intense

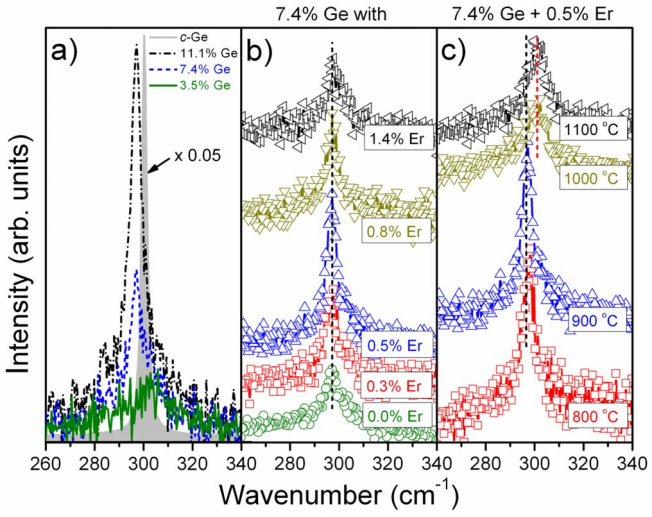

FIG. 1. (Color online) The μ-Raman spectra of the *c* Ge (filled area under the curve in gray) and for the SiO_2 layers containing 3.5, 7.4, and 11.1% Ge, represented by the solid, dashed, and dashed-dot curves, respectively (a); the *c*-Ge data are divided by 20 for clarity. The vertical short dashed lines in both (b) and (c) are the guide to the eyes to follow the peak position with increasing Er concentration and annealing temperature, respectively.

but also downshifted with increasing Ge concentration. It appears at ~ 297.2 cm^{-1} (FWHM ~ 11.3 cm^{-1}). Interestingly, except increasing peak intensity with a subsequent reduction in the linewidth, no further change in frequency position is observed for 11.1% Ge. The mean size of Ge NCs has been estimated to be ~ 6.1, 9.4, and 13.6 nm near R_p by TEM (not shown) for the 3.5, 7.4, and 11.1% Ge, respectively, where the corresponding Ge-Ge Raman peak is expected to be situated at ~ 295, 298.2, and 299 cm^{-1} according to the phonon confinement model.[15] A redshift (~ 5 cm^{-1}) is expected in small crystallites with an average size of ~ 6 nm,[15] which is contrary to the observed blueshift (~ 3.3 cm^{-1}) for 3.5% Ge. In addition, the measured FWHM is comparable to the expected linewidth.[15] As far as the upshift of the 300.2 cm^{-1} peak is concerned, such discrepancy can be due to a dominating role of the compressive strain over the phonon confinement.[15] Based on this concept, we can estimate the magnitude of strain (s) from the measured shift $\Delta\omega \approx 8.5$ cm^{-1} with respect to the calculated position for 3.5% Ge using the relation[15] $\Delta\omega = -s(P+2Q)/2\omega_o$ where $P=-1.3\omega_o^2$ and $Q=-1.65\omega_o^2$ denote the phonon deformation potentials of Ge and ω_o indicates the *c*-Ge peak position. By neglecting the size distribution of Ge NCs, s is estimated to be $\sim 1.23\%$. However, the measured peak position appears at ~ 1.0 cm^{-1} lower than that of the expected frequency[15] for 7.4% Ge. This indicates the presence of a tensile strain along with phonon confinement in crystallites of average size of ~ 9.4 nm. Using $\Delta\omega \approx -1.0$ cm^{-1}, s is estimated to be $\sim 0.14\%$ where the negative sign signifies the tensile strain. It is in good agreement with our XRD results, which will be discussed in the following. In fact, the magnitude of the tensile strain enhances significantly in crystallites with average size of ~ 13.6 nm for 11.1% Ge [see Fig. 1(a)].

Since the Ge-Ge mode is clearly visible for 7.4% Ge, we use it for probing the further development of microstructure in Ge-rich SiO_2 layers with increasing Er concentration (C_{Er}) and annealing temperature (T_a) as exhibited in Figs. 1(b) and 1(c), respectively. Discernibly, instead of any peak shifting, the peak at ~ 297.2 cm^{-1} becomes intensified and sharper with increasing C_{Er} down to FWHM ~ 5.2 cm^{-1} for 0.5% Er, followed by a gradual reduction in intensity by introducing additional Er [Fig. 1(b)]. The corresponding TEM investigations reveal that the average Ge-NC size remains nearly unchanged up to 0.5% Er, while it decreases in size for $C_{Er} > 0.5\%$ due to the sputtering and fragmentation of bigger NCs during Er bombardment. According to the phonon confinement in Ge NCs, broadening and intensity reduction in the Ge-Ge Raman peak are expected with decreasing NC size. This fits with the experimental results for $C_{Er} > 0.5\%$. In order to explain the initial sharpening of the peak with increasing C_{Er} we assume that a part of the implanted Er ions will accumulate in the vicinity of Ge NCs, forming a shell-like structure. In this framework, the phonon wave function is more or less completely confined within Ge NCs before Er doping, whereas the Er ions residing close to Ge NCs may allow a partial propagation of the phonon wave function beyond the NC boundary for 0.3 and 0.5% Er by declining the relaxation condition of the phonon selection rules.[16]

On the other side, the Ge-Ge Raman peak intensity is increased with T_a up to 900 °C, while it drops drastically and moves toward the *c*-Ge peak position [Fig. 1(c)] for $T_a > 900$ °C. RBS measurements reveal that the Ge profile is unaffected during Er implantation, while a significant fraction of Ge is diffused toward the SiO_2/Si and $SiON/SiO_2$ interfaces during Ge-NC formation (not shown). In fact, the diffusion of Ge is accompanied by a gradual reduction in the central Ge peak with increasing T_a without much change in Er profile (Fig. 2). The T_a dependency of the Ge-Ge mode is the result of the following effects: (i) the increase in Ge NC's size with increasing T_a sharpens the peak, while (ii) the diffusion of Ge toward the interfaces followed by the formation of Er phases through segregation of Er located in the surrounding of Ge NCs not only suppresses the peak intensity with a subsequent increase in FWHM but also blueshifts the observed frequency. It is clear from Fig. 1(c) that the second effect dominates for $T_a > 900$ °C. Taking the standard molar Gibbs energy of formation for Er_2O_3 (−1808.7 kJ/mol) and SiO_2 (−856.3 kJ/mol) into account,[17] the subsequent relaxation of the phonon selection rules[16] for higher C_{Er} may be associated with the formation of thermodynamically preferable Er oxide clusters.

This is also revealed from the XRD patterns [Fig. 3(a)], showing the formation of nanocrystallites of Er_2O_3 by introducing 0.8% Er, where the body-centered cubic phase is represented by the (222) and (440) peaks. However, soon after 1.4% Er doping, the Er_2O_3 phase completely disappears. This phenomenon suggests that above 0.8% Er, the Er_2O_3 nanocrystallites are either transformed into an amorphous phase or form a noncrystalline composite structure such as Er-pyrogermanate,[18] depending on the Er to O ratio and the interaction strength in Ge-rich environment. The formation of Ge NCs is, however, indicated by the appearance of the Ge(111) and (220) peaks. The average particle size, S, can be calculated by the Scherrer formula[19] $S = \frac{0.89\lambda}{\beta(2\theta_B)\cdot\cos\theta_B}$ where λ

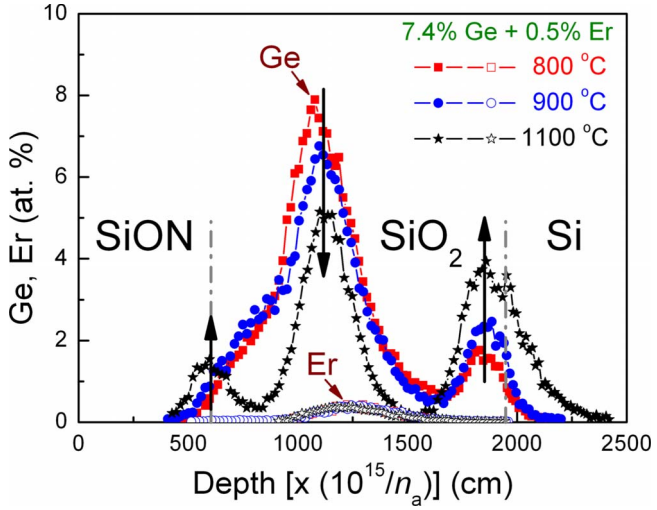

FIG. 2. (Color online) The RBS random spectra, showing the Ge (filled symbols) and Er (open symbols) profiles with increasing T_a for 7.4% Ge and 0.5% Er. The dashed-dotted vertical lines denote the $SiON/SiO_2$ and the SiO_2/Si interfaces. The downward and upward arrows are used to demonstrate the loss of Ge in the central part of the SiO_2 and the segregation of Ge at the interfaces, respectively, with increasing T_a. Taking into account atomic densities (n_a) of 5.00×10^{22}, 6.60×10^{22}, and 6.63×10^{22} at./cm^3 for Si, SiO_2 and SiON, respectively, one can estimate the respective geometric layer thicknesses.

is the x-ray wavelength (0.154 nm) and $\beta(2\theta_B)$ denotes the FWHM of the concerned peak situated at a Bragg angle θ_B. Using this formula, the average NC size is estimated to be ~8.1 nm prior to Er doping, consistent with TEM results (not shown). We can also calculate strain s using the Ge peak position. For the (111) Ge peak, the measured spacing d_0 is ~0.3271 nm. Using the relation[15] $s=(d-d_0)/d_0$ we estimated a tensile strain of ~0.15% where d is the calculated spacing (0.3266 nm) for c Ge. Careful calculation shows that the average NC size decreases from 8.1 down to ~6.4 nm

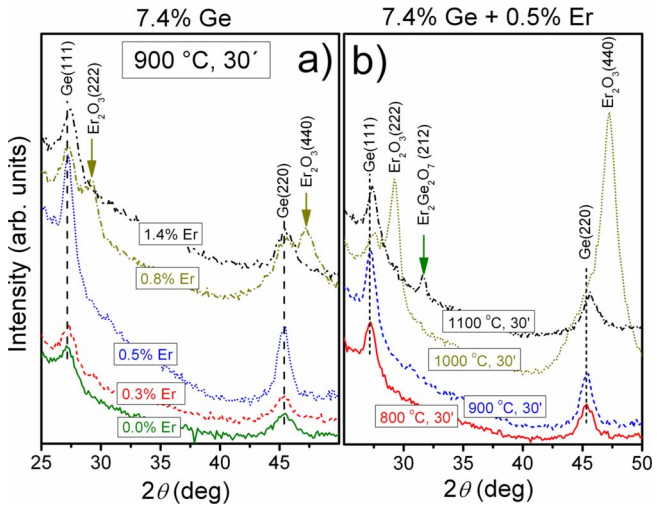

FIG. 3. (Color online) XRD patterns with increasing C_{Er} for 7.4% Ge annealed at 900 °C (a) and with increasing T_a for 7.4% Ge and 0.5% Er (b).

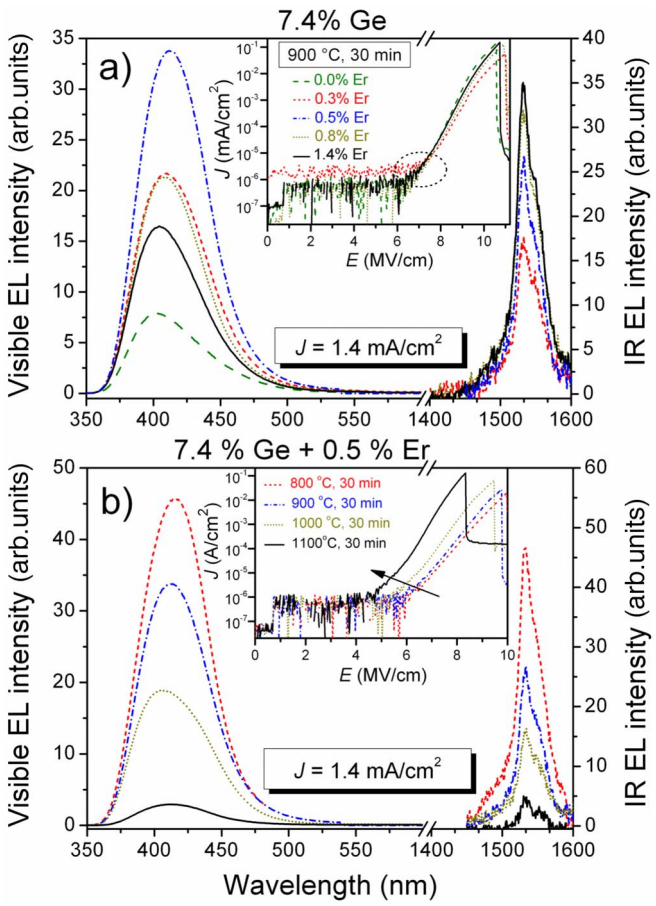

FIG. 4. (Color online) The visible and infrared EL spectra recorded at $J=1.4$ mA/cm^2 with increasing C_{Er} for 7.4% Ge annealed at 900 °C (a) and with increasing T_a for 7.4% Ge and 0.5% Er (b). Note that the scales given in the left and right ordinates in both diagrams (a) and (b) are independent of each other as the signals in the visible and infrared regions were collected by two different detectors. Insets of (a) and (b) show the C_{Er} and T_a dependent modification of the J-E characteristics. The dotted circle represents the unaffected threshold electric field [inset of (a)] with increasing C_{Er}, while the arrow denotes the T_a mediated shifting of the threshold electric field [inset of (b)].

above 0.5% Er, suggesting that the Ge NCs are strongly damaged by high dose Er implantation as a result of a cumulative effect of sputtering, fragmentation, and amorphization processes. Indeed, a significant number of damaged Ge clusters are partially recrystallized (verified by TEM) in the following phase of annealing. In fact, most of the Er ions react strongly with the surrounding oxide matrix during annealing, leading to the development of the Er_2O_3 clusters [Fig. 3(a)] depending on C_{Er}. Interestingly, while the Er oxide precipitates are amorphous in the only Er-doped SiO_2 layers,[20] the Er_2O_3 clusters are crystalline in presence of Ge NCs with average size of ~8.9 nm for 0.8% Er [Fig. 3(a)].

To follow the concerned mechanism with increasing T_a, we also verify the structure by XRD, where the evolution of diffraction patterns is summarized in Fig. 3(b). Following the emergence of the body-centered cubic phase of Er_2O_3 at 1000 °C, the (212) reflection from the $Er_2Ge_2O_7$ nanocrystallites appears at 1100 °C. The tetragonal structure of the

$Er_2Ge_2O_7$ precipitates, which is mainly formed by decomposing Er_2O_3, is known to be noncentrosymmetric and shows anisotropic magnetic properties.[18] Considering the above experimental results, we believe that three basic sources are responsible for controlling the overall structure: (i) liquid-solid phase transition of Ge during high temperature annealing and subsequent interaction with Er ions, (ii) massive diffusion of Ge above the melting point of *c* Ge (~937 °C), and (iii) formation of Er oxide clusters because of extremely low Er solubility in SiO_2 network.[6]

Typical EL spectra for increasing C_{Er} and T_a are displayed in Fig. 4. As evident, each spectrum consists of two clear EL bands with their maxima at ~407 and 1535 nm. While the former one is associated with GeODCs, the latter originates from the intra-$4f$ $^4I_{13/2} \rightarrow {}^4I_{15/2}$ transition in Er^{3+}.[12] Note that the increase in the 407 nm EL intensity as a function of C_{Er} is correlated with the *inverse energy transfer process*.[12] Indeed, the specific amount of Er is crucial for achieving maximum EL yield of the 407 nm peak where it drops significantly above 0.5% Er [Fig. 4(a)]. Bearing in mind the aforementioned structural changes, it is revealed that as long as the Er^{3+} ions are situated in the vicinity of Ge NCs, they can take part in the energy transfer mechanism.[12] For $C_{Er} > 0.5\%$, the inverse energy transfer process is strongly interrupted by the Er bombardment induced structural modification of Ge NCs as well as with Er phase formation. Furthermore, the EL intensity decreases continuously with increasing T_a [Fig. 4(b)], which is in good agreement with the diffusion of Ge toward the SiO_2/Si and $SiON/SiO_2$ interfaces (Fig. 2) and with the formation of the crystalline phases of Er_2O_3 or $Er_2Ge_2O_7$ clusters [Fig. 3(b)].

The current density (J) versus electric field (E) characteristic of the working devices has also been monitored [insets of Figs. 4(a) and 4(b)]. In order to understand the charge injection and transport, measured J-E profiles have been fitted by the conventional mechanisms, namely, Fowler-Nordheim tunneling, Poole-Frenkel emission, hopping mechanism, charging, etc.[20] We found that the Fowler-Nordheim tunneling plays the dominant role. Except little modification in J-E profile, no significant shift in the threshold electric field is observed (indicated by a dashed circle) with increasing C_{Er} [inset of Fig. 4(a)]. This suggests that no change in barrier height occurs at the SiO_2/Si interface by additional Er doping, and hence, the charge injection is almost unaffected. On the contrary, the J-E characteristics shift toward lower electric field (marked by an arrow) with increasing T_a [inset of Fig. 4(b)], which can be assigned to an increase in Ge concentration at the SiO_2/Si interface (Fig. 2) with a concomitant reduction in the barrier height.

In summary, the correlation between the microstructural evolution and the EL properties of the Ge-rich MOS structures codoped with Er has been investigated. It is demonstrated that with increasing C_{Er} up to 0.5%, Er agglomerates in the vicinity of Ge NCs, and promotes the inverse energy transfer process, leading to an increase in the 407 nm EL peak. In fact, 0.5% Er was found to be the optimum value for 7.4% Ge to maximize the 407 nm EL intensity where the formation of Er_2O_3 phase for $C_{Er} > 0.5\%$ diminishes this effect. Moreover, with increasing T_a, the microstructural evolution was characterized by the growth of Ge NCs, the diffusion of Ge toward SiO_2/Si and $SiON/SiO_2$ interfaces, and the formation of Er_2O_3 nanocrystallites followed by the appearance of the $Er_2Ge_2O_7$ phase. All these processes continuously quench the EL signals, and therefore, the annealing at low temperature and/or shorter times is preferable.

Authors thank the Rossendorf Implantation Group for ion implantation and H. Felsmann, C. Neisser, and G. Schnabel for their careful semiconductor preparation work. The support of the Alexander von Humboldt Foundation is gratefully acknowledged.

*a.kanjilal@fzd.de

[1] O. Savchyn, P. G. Kik, R. M. Todi, and K. R. Coffey, Phys. Rev. B **77**, 205438 (2008).
[2] B. Garrido, C. García, S.-Y. Seo, P. Pellegrino, D. Navarro-Urrios, N. Daldosso, L. Pavesi, F. Gourbilleau, and R. Rizk, Phys. Rev. B **76**, 245308 (2007).
[3] I. Izeddin, A. S. Moskalenko, I. N. Yassievich, M. Fujii, and T. Gregorkiewicz, Phys. Rev. Lett. **97**, 207401 (2006).
[4] F. Iacona, D. Pacifici, A. Irrera, M. Miritello, G. Franzò, F. Priolo, D. Sanfilippo, G. Di Stefano, and P. G. Fallica, Appl. Phys. Lett. **81**, 3242 (2002).
[5] G. Z. Ran, Y. Chen, W. C. Qin, J. S. Fu, Z. C. Ma, W. H. Zong, H. Lu, J. Qin, and G. G. Qin, J. Appl. Phys. **90**, 5835 (2001).
[6] J. Lægsgaard, Phys. Rev. B **65**, 174114 (2002).
[7] A. Kanjilal, L. Rebohle, M. Voelskow, W. Skorupa, and M. Helm, J. Appl. Phys. **104**, 103522 (2008).
[8] P. Pellegrino, B. Garrido, J. Arbiol, C. Garcia, Y. Lebour, and J. R. Morante, Appl. Phys. Lett. **88**, 121915 (2006).
[9] C. Bulutay, Phys. Rev. B **76**, 205321 (2007).
[10] S. Decoster, B. De Vries, U. Wahl, J. G. Correia, and A. Vantomme, Appl. Phys. Lett. **93**, 141907 (2008).
[11] C. L. Heng, T. G. Finstad, P. Storås, Y. J. Li, and A. E. Gunnæs, Appl. Phys. Lett. **85**, 4475 (2004).
[12] A. Kanjilal, L. Rebohle, M. Voelskow, W. Skorupa, and M. Helm, Appl. Phys. Lett. **94**, 051903 (2009).
[13] J. F. Zeigler, SRIM-2006.02 (http://www.srim.org).
[14] A. Janotta, M. Schmidt, R. Janssen, M. Stutzmann, and Ch. Buchal, Phys. Rev. B **68**, 165207 (2003).
[15] X. L. Wu, T. Gao, X. M. Bao, F. Yan, S. S. Jiang, and D. Feng, J. Appl. Phys. **82**, 2704 (1997).
[16] A. K. Arora, M. Rajalakshmi, T. R. Ravindran, and V. Sivasubramanian, J. Raman Spectrosc. **38**, 604 (2007).
[17] *CRC handbook of Chemistry and Physics*, edited by D. R. Lide (CRC, Boca Raton, FL, 2006).
[18] E. Morosan, J. A. Fleitman, Q. Huang, J. W. Lynn, Y. Chen, X. Ke, M. L. Dahlberg, P. Schiffer, C. R. Craley, and R. J. Cava, Phys. Rev. B **77**, 224423 (2008).
[19] H. Ninomiya, N. Itoh, S. Rath, S. Nozaki, and H. Morisaki, J. Vac. Sci. Technol. B **17**, 1903 (1999).
[20] A. Kanjilal, L. Rebohle, W. Skorupa, and M. Helm, Appl. Phys. Lett. **94**, 101916 (2009).